The Astrophysical Journal, 798:10 (11pp), 2015 January 1 doi:10.1088/0004-637X/798/1/10


# GRB 130427A AND SN 2013cq: A MULTI-WAVELENGTH ANALYSIS OF AN INDUCED GRAVITATIONAL COLLAPSE EVENT

R. Ruffini[1,2,3,4], Y. Wang[1,2], M. Enderli[1,3], M. Muccino[1,2], M. Kovacevic[1,3], C. L. Bianco[1,2], A. V. Penacchioni[4], G. B. Pisani[1,3], and J. A. Rueda[1,2,4]

[1] Dip. di Fisica and ICRA, Sapienza Università di Roma, Piazzale Aldo Moro 5, I-00185 Rome, Italy
[2] ICRANet, Piazza della Repubblica 10, I-65122 Pescara, Italy; yu.wang@icranet.org
[3] Université de Nice Sophia Antipolis, CEDEX 2, Grand Château Parc Valrose, Nice, France
[4] ICRANet-Rio, Centro Brasileiro de Pesquisas Fisicas, Rua Dr. Xavier Sigaud 150, Rio de Janeiro, RJ 22290-180, Brazil
*Received 2014 March 7; accepted 2014 October 17; published 2014 December 11*

## ABSTRACT

We performed a data analysis of the observations by the *Swift*, *NuStar*, and *Fermi* satellites in order to probe the induced gravitational collapse (IGC) paradigm for gamma-ray bursts (GRBs) associated with supernovae (SNe) in the terra incognita of GRB 130427A. We compare our data analysis with those in the literature. We have verified that GRB 130427A conforms to the IGC paradigm by examining the power law behavior of the luminosity in the early $10^4$ s of the XRT observations. This has led to the identification of the four different episodes of the binary driven hypernovae (BdHNe) and to the prediction, on 2013 May 2, of the occurrence of SN 2013cq, which was also observed in the optical band on 2013 May 13. The exceptional quality of the data has allowed the identification of novel features in *Episode 3* including: (1) the confirmation and the extension of the existence of the recently discovered nested structure in the late X-ray luminosity in GRB 130427A, as well as the identification of a spiky structure at $10^2$ s in the cosmological rest-frame of the source; (2) a power law emission of the GeV luminosity light curve and its onset at the end of *Episode 2*; and (3) different Lorentz $\Gamma$ factors for the emitting regions of the X-ray and GeV emissions in this *Episode 3*. These results make it possible to test the details of the physical and astrophysical regimes at work in the BdHNe: (1) a newly born neutron star and the supernova ejecta, originating in *Episode 1*; (2) a newly formed black hole originating in *Episode 2*; and (3) the possible interaction among these components, observable in the standard features of *Episode 3*.

*Key words:* black hole physics – gamma-ray burst: general – nuclear reactions, nucleosynthesis, abundances – stars: neutron – supernovae: general

## 1. INTRODUCTION AND SUMMARY OF PREVIOUS RESULTS

That some long gamma-ray bursts (GRBs) and supernovae (SNe) can occur almost simultaneously has been known since the early observations of GRB 980425/SN 1998bw (Galama et al. 1998; Pian et al. 2000). This association of a GRB and an SN occurs most commonly in a family of less energetic long GRBs with the following characteristics: (1) isotropic energies $E_{\rm iso}$ in the range of $10^{49}$–$10^{52}$ erg (Guetta & Della Valle 2007); (2) a soft spectrum with rest-frame peak energy $E_{p,i} < 100$ keV, although the instruments are sensitive up to GeV; and (3) supernova emissions observable up to a cosmological distance $z < 1$. Hereafter we will refer to this family as *family 1*. This is well recognized in the literature; see, e.g., (Maselli et al. 2014).

An alternative family of highly energetic long GRBs that are associated with SNe and that has a much more complex structure exists. Their characteristics are: (1) $E_{\rm iso}$ is in the range $10^{52}$–$10^{54}$ erg; (2) they present multiple components in their spectra and in their overall luminosity distribution, ranging from X-ray to $\gamma$-ray all the way to GeV emission. They have peak energies from 100 keV to some MeV; (3) in view of their large energetics, their observation extends to the entire universe all the way up to $z = 8.2$ (Ruffini et al. 2014b). Hereafter we will refer to this family as *family 2*.

There was some doubt that SNe may be associated with very bright long GRBs. Naive energetic arguments said it was unlikely for an SN to be in a powerful GRB within the single star collapse model (see e.g., Maselli et al. 2014).

For some years the issue of the coincidence of very energetic GRBs with SN has represented an authentic terra incognita. It is critical to clarify whether this association of GRBs and SNe is only accidental or if it is necessary, independent of their energetics. Of the 104 long GRBs with known redshift $z < 1$, 19 GRBs associated with SNe belonging to the *family 2* were observed (Kovacevic et al. 2014) before 2014 June, and GRB 130427A, with isotropic energy $E_{\rm iso} \simeq 10^{54}$ erg, is the most energetic one so far.

In Ruffini et al. (2001, 2008) we introduced the paradigm of induced gravitational collapse (IGC) to explain the astrophysical reasons for the association of GRBs with supernovae. This paradigm indicates that all long GRBs, by norm, must be associated with SNe. The IGC paradigm differs from the traditional collapsar–fireball paradigm (see, e.g., Piran 2005 and references therein). In the collapsar–fireball model, the GRB process is described by a single episode: (1) it is assumed to originate in a "collapsar" (Woosley 1993), (2) the spectral and luminosity analysis is typically time integrated over the entire $T_{90}$ (see e.g., Tavani 1998), and (3) the description of the afterglow is dominated by a single ultra-relativistic jetted emission (see, e.g., in Rhoads 1999; van Eerten et al. 2010; van Eerten & MacFadyen 2012; Nava et al. 2013). In contrast, the IGC paradigm considers a multi-component system, similar to those described by *S*-matrix in particle physics, as shown in Figure 1: (1) the in-states are represented by a binary system formed by an FeCO core, which is very close to the onset of an SN event and a tightly bound companion neutron star (NS; Ruffini et al. 2008; Rueda & Ruffini 2012; Izzo et al. 2012). The out-states are the creation of a new NS ($\nu$-NS) and black hole

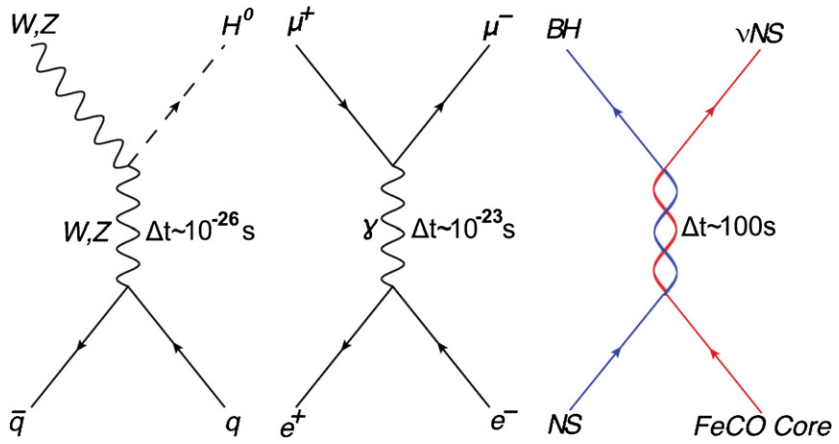


**Figure 1.** Three different matrices in fundamental physics. The first is the quark matrix leading to a Higgs boson. The middle is the classical electron–positron pair matrix, generating a muon and anti-muon pair. The third matrix is the most recent and it is considered in the present work. $\Delta t$ is the duration of the intermediate state.

(BH). In the case of particle physics, the *S*-matrix describes a virtual phenomenon occurring on timescales of $10^{-26}$ s (Aad et al. 2012, $q\bar{q} \rightarrow WZH^0$) and $10^{-23}$ s (Bernardini 2004, $e^+e^- \rightarrow \mu^+\mu^-$). In the astrophysical case considered here, the cosmic matrix (*C*-matrix) describes a real event occurring on timescale ~200 s, which is still a very short time when compared to traditional astrophysical timescales. Following the accretion of the SN ejecta onto the companion NS binary, a BH is expected to be created, giving rise to the GRB. (2) Special attention is given to the analysis of the instantaneous spectra in the optical, X-ray, $\gamma$-ray, and GeV energy range (as exemplified in this article). (3) Four different episodes are identifiable in the overall emission, each with marked differences in the values of their Lorentz $\Gamma$ factors (Ruffini et al. 2014c). The possible relevance of a binary system in the explanation of GRBs was already mentioned by Fryer et al. (1999) and Broderick (2005), but the binaries were a trigger to the traditional collapsar model.

The opportunity to probe the IGC paradigm (Izzo et al. 2012) comes from the prototypical source GRB 090618, which is a member of *family 2*. This source has extremely high energetics (i.e., $E_{\rm iso} = 2.7 \times 10^{53}$ erg), is at a relatively close distance (i.e., $z = 0.54$), and has coverage in all existing $\gamma$, X-ray, and optical observatories.

The following results have been obtained (see visualized spacetime diagram in Figure 2):

1. *Episode 1*, which corresponds to the onset of the SN and the accretion process onto the companion NS, was identified in the early 1950 s, with a thermal plus power law component in the spectra (see Izzo et al. 2012, Figure 16), as well as a temporal evolution of the radius of the emitting region expanding from $10^9$ cm to $7 \times 10^9$ cm (see Izzo et al. 2012, Figure 18). This leads to a precise determination of its overall energetics of $4 \times 10^{52}$ erg.
2. *Episode 2*, with the GRB emission, follows the onset of gravitational collapse and the BH formation. It was also clearly identified with the following characteristic parameters: an isotropic energy $E_{\rm iso} = 2.49 \times 10^{53}$, baryon loading $B = 1.98 \times 10^{-3}$, Lorentz factor $\Gamma = 495$ (see Izzo et al. 2012, Figure 4), and peak energy $E_{p,i} = 193$ keV. The average number density of the circumburst medium (CBM) is $\langle n_{\rm CBM} \rangle = 0.6\,{\rm cm}^{-3}$. The characteristic masses of each CBM cloud are of the order ~$10^{22}$–$10^{24}$ g, at $10^{16}$ cm in radii (see Izzo et al. 2012, Figure 10).
3. *Episode 3* of GRB 090618, detected by *Swift*-XRT, starts at 150 s after the burst trigger and continues all the way up to $10^6$ s. It consists of three different parts (Nousek et al. 2006): a first very steep decay; a shallower decay, the plateau; and a final steeper decay with a fixed power law index. It soon became clear that *Episode 3*, which was

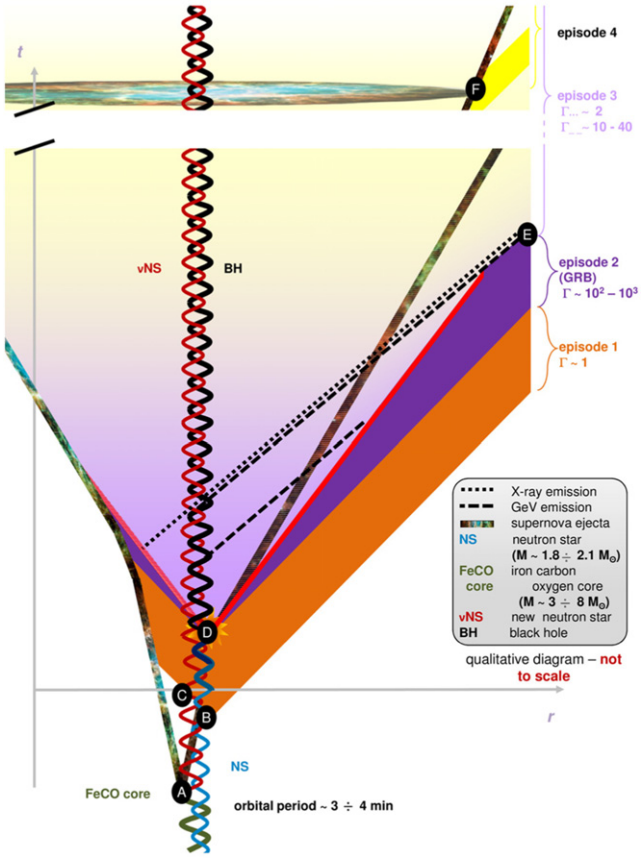


**Figure 2.** IGC spacetime diagram (not in scale) illustrates four episodes of the IGC paradigm: the nonrelativistic *Episode 1* ($\Gamma \simeq 1$), the relativistic motion of *Episode 2* ($\Gamma \simeq 10^2 \sim 10^3$), the mildly relativistic *Episode 3* ($\Gamma \simeq 2$), and nonrelativistic *Episode 4* ($\Gamma \simeq 1$). There is initially a binary system composed of a massive star (yellow thick line) and a neutron star (blue line). The massive star evolves and explodes as an SN at point A, forming a $\nu$NS (red line). The companion NS accretes the supernova ejecta starting from point B, interacts with the $\nu$NS starting from point C, and collapses into a black hole (black line) at point D; this period from point B to point D is defined as *Episode 1*. Point D is the beginning of *Episode 2*, which is caused by the collision of GRB outflow and interstellar filaments. At point E, *Episode 2* ends and *Episode 3* starts, lasting until the optical signal of the supernova emerges at point F, where *Episode 4* starts. (*Credit to M. Enderli for drawing this visualized spacetime diagram.*)

previously interpreted in the traditional approach as part of the GRB afterglow (Piran 2005; Rhoads 1999; van Eerten et al. 2010; van Eerten & MacFadyen 2012; Nava et al. 2013), appeared to be the seat of a set of novel independent processes occurring after the end of the GRB emission and preceding the optical observation of the SN, which we indicated as *Episode 4*.

Progress has recently been made in the analysis of *Episode 1*. It is characterized by the explosion of the FeCO core, followed by the hypercritical accretion onto the NS, which leads to the NS reaching critical mass and consequently its induced gravitational collapse to a BH. The hypercritical accretion of the SN ejecta onto the NS has been estimated using the Bondi–Hoyle–Lyttleton formalism to be $10^{-2}\,M_{\odot}\,\mathrm{s}^{-1}$; here $M_{\odot}$ is the solar mass (Bondi & Hoyle 1944; Bondi 1952) (see, e.g., in Rueda & Ruffini 2012). The inflowing material shocks as it piles up onto the NS, producing a compressed layer on top of the NS (see, e.g., Fryer et al. 1996). As this compressed layer becomes sufficiently hot, it triggers the emission of neutrinos that cool the infalling material, allowing it to be accreted into the NS (Zel'dovich et al. 1972; Ruffini & Wilson 1975; Ruffini et al. 1999, 2000; Fryer et al. 1996, 1999). Recently Fryer et al. (2014) presented significant progress in understanding the underlying physical phenomena in the aforementioned hypercritical accretion process of the supernova ejecta into the binary companion neutron star (Ruffini et al. 2008; Rueda & Ruffini 2012). The new treatment, based on the two-dimensional cylindrical geometry smooth particle hydrodynamics code, has numerically simulated the process of hypercritical accretion—the classical Bondi–Hoyle regimes—in the specific case of the IGC paradigm, and led to the first astrophysical application of the neutrino production process considered in Zel'dovich et al. (1972) and in Ruffini & Wilson (1975; see e.g., in R. Ruffini et al., presentation in the Zeldovich-100 meeting)[5]. Indeed the fundamental role of neutrinos' emission allows the accretion rate process to increase the mass of the binary companion star to its critical value, which leads to the black hole formation giving rise to the GRB in *Episode 2*. These results confirm and quantify the general considerations presented in Rueda & Ruffini (2012).

In *Episode 2* all technical, numerical, and basic physical processes have been tested in the literature, and the fireshell model is now routinely applied to all GRBs (see, e.g., GRB 101023 in Penacchioni et al. 2012 and GRB 110709B in Penacchioni et al. 2013).

The main aim of this paper is dedicated to a deeper understanding of the physical and astrophysical process present in *Episode 3*:

1. to give evidence of the universal properties of *Episode 3* observed in additional sources belonging to *family 2*, as compared to the very high variability of *Episode 1* and *Episode 2* components;
2. to present observations of GRB130427A leading to identification of new physical regimes encountered in *Episode 3* and their interpretation within the IGC paradigm;
3. to give evidence of the predictive power of the observations of *Episode 3* and outline the underlying physical process leading to the characterization of the two aforementioned families of GRBs.

[5] http://www.icranet.org/index.php?option=com_content&task=view&id=747&Itemid=880

To start we will summarize in the next paragraph some qualifying new features generally observed in *Episode 3* of selected GRBs of *Family 2* and proceed in the following paragraphs to the specific new information acquired about *Episode 3* from GRB 130427A. We will then proceed to the general conclusions.

## 2. THE QUALIFYING FEATURES OF *EPISODE 3*

As observations of additional sources fulfilling the IGC paradigm were performed, some precise qualifying features for characterizing *Episode 3* have been found.

1. In some GRBs with known redshift belonging to *family 2* the late X-ray luminosities at times larger than $10^4$ s appeared to overlap when duly scaled in the proper rest frame of the GRB source (Penacchioni et al. 2012). This was soon confirmed for a sample of six GRBs (i.e., GRB 060729, GRB 061007, GRB 080319B, GRB090618, GRB 091127, and GRB 111228), which we call the golden sample (*GS*; Pisani et al. 2013); see Figure 3. This unexpected result led to the adoption of the universal luminosity versus time relation in the late X-ray emission of *Episode 3* as a distance indicator. For some GRBs without a known cosmological redshift and exhibiting the general features of the four episodes, we imposed the overlapping of the late power law X-ray emission in *Episode 3* with those of the *GS*, and consequently we inferred the value of the cosmological redshift of the source. This led to inferring the overall energetics of the source and a consistent description of each episode following our theoretical model. This was the case with GRB 101023, which has an inferred redshift $z = 0.9$ and $E_{\rm iso} = 4.03 \times 10^{53}$ erg (Penacchioni et al. 2012), and GRB 110709B, with inferred redshift $z = 0.75$ and $E_{\rm iso} = 2.43 \times 10^{52}$ erg (Penacchioni et al. 2013).

   The above analysis initially addressed sources with $z < 1$, where the associated SNe are observable. However, there is no reason to doubt that the IGC paradigm also applies to sources for $z > 1$. In this case the SN is not observable with the current optical telescopes, but the existence of all the above episodes, with the exception of *Episode 4* related to the optical observation of the SN, can be verified in principle if they are above the observational threshold, and the members of the *GS* are correspondingly further increased. Indeed, significant results have been reached by observing the fulfillment of the above scaling laws in *Episode 3* of GRB 090423, at $z = 8.2$ (Ruffini et al. 2014b). The occurrence of this overlapping in the late X-ray emission observed by XRT is considered a necessary and sufficient condition to assert that a GRB fulfills the IGC paradigm.
2. The identification of a thermal emission occurring in the initial very steep decay of *Swift*-XRT data of *Episode 3* in GRB 090618 (Ruffini et al. 2014c). We are currently examining other GRBs with this feature, e.g., 060729, 061007, 061121 (Page et al. 2011; Starling et al. 2012; Friis & Watson 2013). From these thermal emissions it is possible to infer the dimensions of the X-ray emitting regions, as well as their Lorentz $\Gamma$ factors, in this earliest part of *Episode 3* (Ruffini et al. 2014c). A typical mildly relativistic expansion regime with $\Gamma \lesssim 2$ and characteristic radii $R \sim 10^{13}$ cm has been identified (Ruffini et al. 2014c). These observational facts lead to a novel approach to the theoretical understanding of the X-ray emission

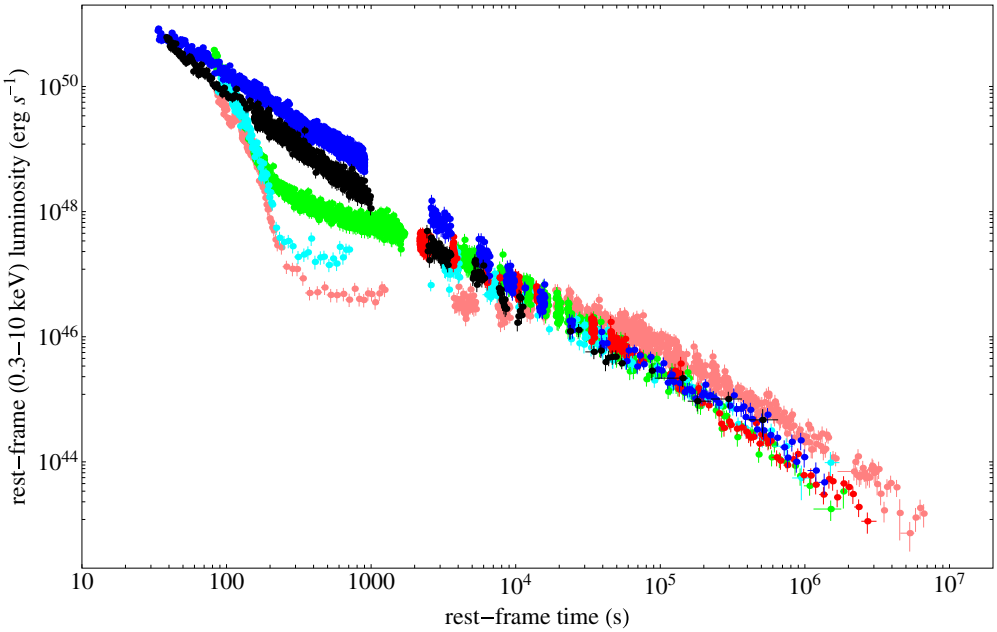


**Figure 3.** Golden sample scaling law (Pisani et al. 2013). X-ray luminosity light curves of the six GRBs with measured redshift in the 0.310 keV rest-frame energy range: in pink GRB 060729, $z = 0.54$; black GRB 061007, $z = 1.261$; blue GRB 080319B, $z = 0.937$; green GRB 090618, $z = 0.54$; red GRB 09112 7, $z = 0.49$; and in cyan GRB 111228, $z = 0.713$.

process of *Episode 3*, which is profoundly different from the ultra-relativistic one in the traditional jet afterglow collapsar paradigm model (Piran 2005; Mészáros 2006). We concluded that this emission is not only mildly relativistic, but also linked to a wide-angle emission from the SN ejecta in the absence of any sign of collimation (Ruffini et al. 2014c).

3. From the direct comparison of the late X-ray emission of the *GS* sources, we recently identified the appearance of a nested structure, which we illustrate in Figure 4, comparing the corresponding behavior of GRB 130427A with that of *GS* GRB 060729 (Ruffini et al. 2014c). The occurrence of these nested structures shows, among others, that in the case of the most intense sources, the common power law observed for the X-ray luminosities for times larger than $10^4$ s does extend to earlier times; see Figure 4. Indeed, for the most intense sources, the common power law behavior is attained at an earlier time and at higher X-ray luminosities than the characteristic timescale indicated in (Pisani et al. 2013); see Figure 3. As we are going to show, in the highly energetic GRB 130427A, this behavior starts at much earlier times around 400 s.

Some of these results were presented by one of the authors in the 2013 Texas Symposium on Relativistic Astrophysics.[6] There, the sources originating in a tight binary system composed of a FeCO core at the onset of an SN event and a companion NS were named binary driven hypernovae (BdHNe; Ruffini et al. 2014c), in order to distinguish them from the traditional hypernovae (HN).

The occurrence of the three features of *Episode 3* listed previously as obtained by our data analysis are becoming crucial to the theoretical understanding of the GRB–SN phenomenon. They have never been envisaged to exist or predicted in the traditional collapsar–fireball paradigm (Nava et al. 2013; van Eerten & MacFadyen 2012; van Eerten et al. 2010). The IGC paradigm motivated an attentive data analysis of *Episode 3* and the discovery of its universality has been a by-product.

[6] http://nsm.utdallas.edu/texas2013/proceedings/3/1/Ruffini.pdf

## 3. *EPISODE 3* IN THE CASE OF GRB 130427A

In what follows we will show how GRB 130427A, which is associated with SN 2013cq and is the most luminous GRB observed in the past 40 yr, offers the longest multi-wavelength observations of *Episode 3* so far. It confirms and extends the above understanding and corresponding scaling laws already observed in X-rays to lower and higher energies. It also allows for the exploration of the occurrence of similar constant power law emission in the high-energy emission (GeV) and in the optical domain. We proceed with our data analysis of the ultra high GeV energy observations (*Fermi*-LAT), those in soft and hard X-rays (*Swift*-XRT and *NuStar*, respectively), as well as of optical observations (*Swift*-UVOT and ground based satellites). Our results are compared to those in the current literature. These observational facts set very specific limits on the Lorentz $\Gamma$ factor of each component; the corresponding mechanism of emission; and the clear independence of any prolongation of the GRB emission of *Episode 2* to the emission process of *Episode 3*.

The observation of the scaling law in the first $2 \times 10^4$ s alone has allowed us to verify the BdHN nature of this source, which necessarily implies the presence of a SN. Consequently, we recall in Section 3.1 that we made the successful prediction of the occurrence of a supernova, which was observed in the optical band, as predicted on 2013 May 2.

In Section 3.2, we summarize our own data reduction of the *Fermi* and *Swift* satellites, and we compare them with those in the current literature.

In Section 3.3, we discuss the finding of a thermal component in the early part of the X-ray emission of *Episode 3*. This is crucial for identifying the existence of the X-ray emission of a regime with low Lorentz factor and small radius, which is typical for supernova ejecta.

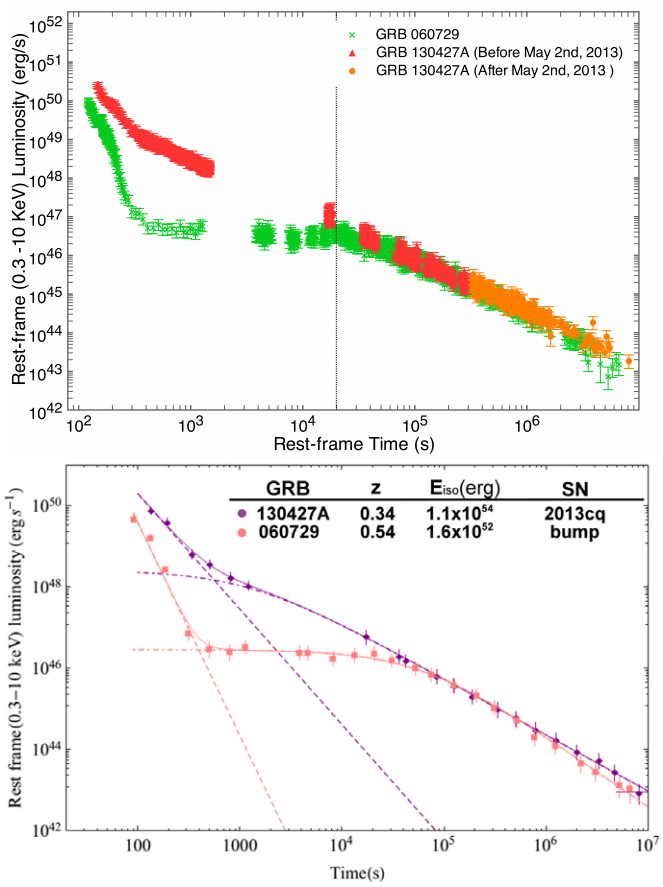


**Figure 4.** Top: overlapping of GRB 130427A and GRB 060729. The green crosses represent the light curve of GRB 060729. The red triangle and orange dots represent the light curve of GRB 130427A before and after 2013 May 2, respectively. The vertical line marks the time of $2 \times 10^4$ s, which is the lower limit for the domain of validity of the Pisani relation prior to GRB 130427A. Bottom: this figure shows that GRB 060729 and GRB 130427A have different magnitudes of the isotropic energy, but exhibit a common scaling law after $2 \times 10^4$ s. It also shows that the low isotropic energy GRB 060729 has a longer plateau, while the high isotropic energy GRB 130427A does not display an obvious plateau.

In Section 3.4 we compare the broadband (optical, X-ray, $\gamma$-ray, all the way up to GeV) light curves and spectra of *Episode 3*.

In Section 3.5 we point out the crucial difference between the X-, $\gamma$-ray, and GeV emission in *Episode-3*.

In Section 3.6 we proceed to a few general considerations on ongoing theoretical activities.

Sections 4 is the summary and conclusions.

### 3.1. Identification and Prediction

With the appearance of GRB 130427A, we decided to explore the applicability of the IGC paradigm in the terra incognita of GRB energies up to $\sim 10^{54}$ erg. In fact, prior to GRB 130427A, the only known case of an equally energetic source, GRB 080319B, had some evidence of an optical bump (Bloom et al. 2009; Tanvir et al. 2010), but in no way gave detailed information about the SN spectrum or type. We noticed in GRB 130427A the characteristic overlapping of the late X-ray decay in the cosmological rest frame of the source with that of GRB 060729, a member of the golden sample (in red in Figure 4), and from the overlapping we deduced a redshift that was consistent with the observational value $z = 0.34$ (Levan et al. 2013a).

Therefore from the observations of the first $2 \times 10^4$ s, GRB 130427A fulfilled the IGC paradigm, and we conclude, solely on this ground, that an SN should be observed under these circumstances. We sent the GCN circular 14526[7] (Ruffini et al. 2013b) on 2013 May 2 predicting that the optical *R*-band of an SN will reach its peak magnitude in about 10 days in the cosmological rest frame on the basis of the IGC paradigm. Starting from 2013 May 13 the telescopes GTC, Skynet, and HST discovered the signals from the type Ic supernova SN 2013cq (de Ugarte Postigo et al. 2013; Trotter et al. 2013; Levan et al. 2013b, 2014; Xu et al. 2013). We kept updating the X-ray *Swift* data for weeks and confirmed the complete overlapping of the late X-ray luminosities, in the respective cosmological rest frames, of GRB 130427A and GRB 060729 (in orange in Figure 4). From these data it became clear that the power law behavior of the late-time X-ray luminosity with index $\alpha \sim 1.3$ indicated in Pisani et al. (2013)—leading to the new concept of the nesting of the light curves—started in this very energetic source at $\sim 10^2$ s following an initial phase of steeper decay (Ruffini et al. 2014c).

Contrary to the traditional approach that generally considers a GRB to be composed of the prompt emission followed by the afterglow, both of which vary from source to source, the IGC paradigm for *family 2* introduced *Episode 3,* which shows regularities and standard late-time light curves that are largely independent of the GRB energy. It soon became clear that, with *Episode 3*, we were starting to test the details of the physics and astrophysics of as yet unexplored regimes implied by the IGC paradigm: (1) a $\nu$-NS and the SN ejecta, originating in *Episode 1*, (2) a newly formed BH originating in *Episode 2*, and (3) the possible interaction among these components observable in the standard features of *Episode 3*.

The joint observations of the *Swift*, *NuStar*, and *Fermi* satellites have offered the unprecedented possibility of clarifying these new regimes with the addition of crucial observations in the optical, X-ray, and high energy radiation for *Episode 3* of GRB 130427A, leading to equally unexpected results. The remainder of this paper is dedicated to understanding *Episode 3* of this remarkable event.

### 3.2. Data Analysis of Episode 3 in GRB 130427A

GRB 130427A was first observed by the *Fermi*-GBM at 07:47:06.42 UT on 2013 April 27 (von Kienlin 2013), which we set as the starting time $t_0$ throughout the entire analysis. After 51.1 s, the Burst Alert Telescope (BAT) on board *Swift* was triggered. The *Swift* Ultra Violet Optical Telescope (UVOT) and the *Swift* X-ray Telescope (XRT) began observing at 181 s and 195 s after the GBM trigger, respectively (Maselli et al. 2013). Because this was an extremely bright burst, successively more telescopes pointed at the source: the Gemini North telescope in Hawaii (Levan et al. 2013a), the Nordic Optical Telescope (NOT) (Xu et al. 2013), and the VLT/X-shooter (Flores et al. 2013), which confirmed the redshift $z = 0.34$.

[7] GCN 14526: the late X-ray observations of GRB 130427A by *Swift*-XRT clearly show a pattern typical of a family of GRBs associated with supernovae (SNe), following the Induced Gravitational Collapse (IGC) paradigm (Rueda & Ruffini 2012; Pisani et al. 2013). We assume that the luminosity of the possible SN associated with GRB 130427A would be that of 1998bw, as was found in the IGC sample described in Pisani et al. (2013). Assuming the intergalactic absorption in the *I* band (which corresponds to the *R*-band rest frame) and the intrinsic one, with a Milky Way type for the host galaxy, we obtain a magnitude expected for the peak of the SN of $I = 22$–$23$ occurring 13–15 days after the GRB trigger, namely between the 10th and the 12th of 2013 May. Further optical and radio observations are encouraged.

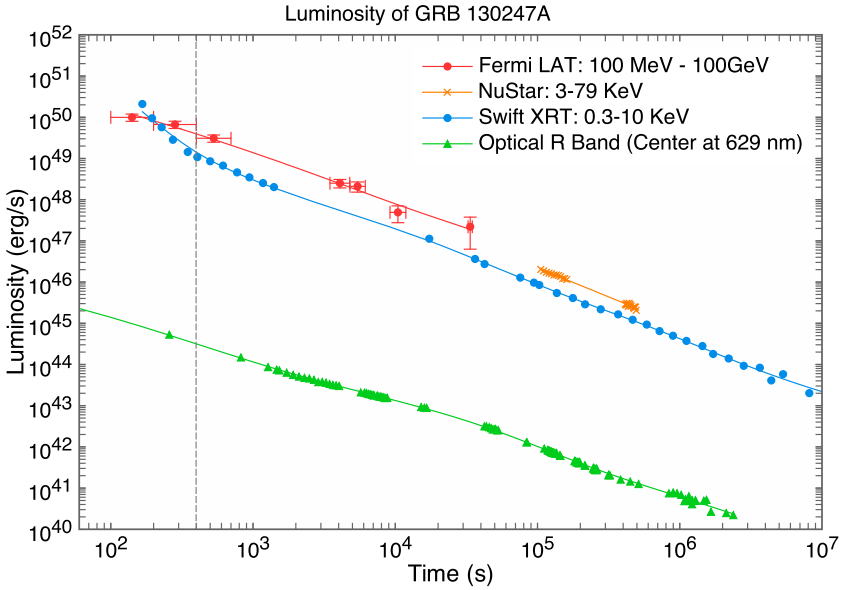


**Figure 5.** Multi-wavelength light curve of GRB 130427A. The high energy (100 MeV–100 GeV) emission detected by *Fermi*-LAT marked in red, and soft X-ray (0.3–10 keV) data from *Swift*-XRT marked in blue, are deduced from the original data. *NuStar* data (3–79 keV) marked in orange comes from (Kouveliotou et al. 2013). The optical (*R*-band, center at 629 nm) data marked in green comes from ground-based instruments (Perley et al. 2013). The error bars are too small with respect to the data points except for *Fermi*-LAT data. The horizontal error bars of *Fermi*-LAT represent the time bin in which the flux is calculated and vertical bars are statistical $1\sigma$ errors on the flux (the systematic error of 10% is ignored). The details in the first tens of seconds are ignored because we are interested in the behavior of the high energy light curve on a longer time scale. The vertical gray dashed line at (~400 s) indicates when the constant decaying slope starts. It is clear that all the energy bands have almost the same slope after 400 s in *Episode 3*.

GRB 130427A is one of the few GRBs with an observed adequate fluence in the optical, X-ray, and GeV bands simultaneously for hundreds of seconds. In particular it remained continuously in the LAT field of view until 750 s after the trigger of *Fermi*-GBM (Ackermann et al. 2013), which gives us the best opportunity so far to compare the light curves and spectra in different energy bands, and to verify our IGC paradigm. We did the data reduction of *Fermi* and *Swift* satellites using the following methods.

*Fermi*. Data were obtained from the Fermi Science Support Center,[8] and were analyzed using an unbinned likelihood method with Fermi Science Tools v9r27p1.[9] Event selections $P7SOURCE\_V6$ and $P7CLEAN\_V6$ were used, depending on which one gave more stable results. Recommended data cuts were used (e.g., $z_{\max} = 100$ degree). The background is composed of the galactic diffuse emission template and the isotropic emission template, as well as about 60 point sources that are within the 15° radius of the GRB (however, their contribution was found to be negligible). The parameters for the background templates were held fixed during the fit. Luminosity light curve in Figure 5 corresponds to the energy range of 100 MeV to 100 GeV, a circle radius of 15°, with a power law spectra assumption. Because the data points up to the last two give a photon index of $\simeq$2.1 with small errors, we set the photon index for the last two points to the value 2.1 during the fitting procedure in order to obtain more stable results. The light curve can be obtained with great temporal detail before 750 s. However, because we are interested in the general behavior of *Episode 3*, for simplicity we neglected such a fine temporal structure and rebinned the light curve. Therefore there are only three data points up to 750 s. The spectrum is plotted in Figure 6.

*Swift*. XRT data were retrieved from UKSSDC[10] and were analyzed by the standard *Swift* analysis software included in the NASA's Heasoft 6.14 with relevant calibration files.[11] In the first 750 s only Windows Timing (WT) data exists and the average count rate exceeds 300 counts $s^{-1}$; the highest count rate reaches up to 1000 counts $s^{-1}$, which is far beyond the value of 150 counts $s^{-1}$ that is suggested for the WT mode as a threshold of considering pile-up effects (Evans et al. 2007). Pile-up effects cause the detector to misrecognize two or more low energy photons as a single high energy photon, which softens the spectrum. We adopted the method proposed by Romano et al. (2006), fitting dozens of spectra from different inner sizes of box annulus selections in order to determine the extent of the distorted region. Taking the time interval 461–750 s as an example, the deviation comes from where the inner size is smaller than six pixels, as shown in Figure 6. Then we applied the standard XRT data analyzing process (Evans et al. 2007, 2009) to obtain the spectrum, as plotted in Figure 6. For the luminosity light curve we split XRT observations in the nominal 0.3–10 keV energy range to several slices with a fixed count number, followed the standard procedure (Evans et al. 2007, 2009), and considered the pile-up correction. The XRT light curves of different bands are shown in Figure 5.

### 3.3. The X-Ray Qualification of GRB 130427A as a BdHN

Here we first focus on the extended X-ray emission of *Episode 3*, which, as shown, gives the qualifying features for the identification of GRB 130427A as a BdHN. We first identify the power law component of the light curve after the steep decay and the end of the plateau. This power law component of GRB 130427A has a power law index $\alpha = -(1.31 \pm 0.01)$ and extends from 400 s to $\sim 10^7$ s without jet breaks. These results are consistent with previous papers (see, e.g., in Perley

[8] http://Fermi.gsfc.nasa.gov
[9] http://Fermi.gsfc.nasa.gov/ssc/data/analysis/software/
[10] http://www.Swift.ac.uk
[11] http://heasarc.gsfc.nasa.gov/lheasoft/

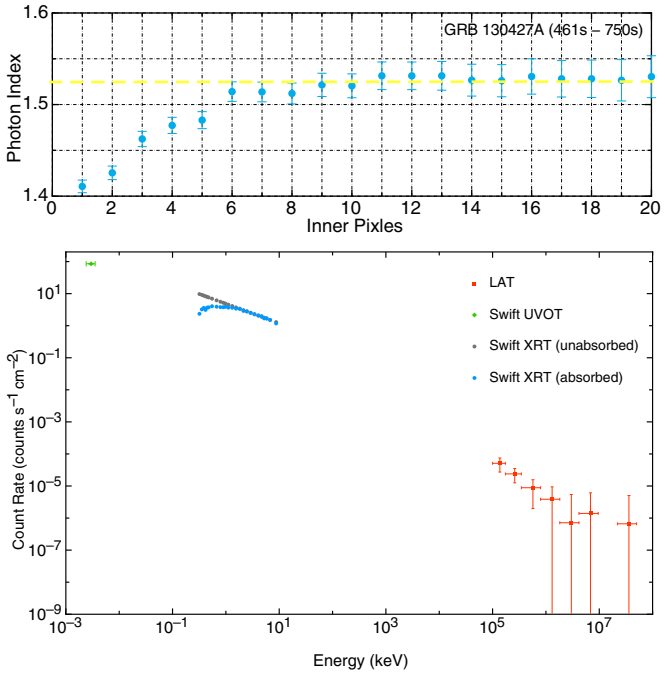


**Figure 6.** Top: data from the *Swift*-XRT (0.3–10 keV) in the time range of 461–750 s for GRB 130427A. The data shows the photon index for different region selections after considering the pile-up effect. After six inner pixels, the photon index approaches an almost constant value of 1.52. Bottom: spectra of GRB 130427A in the time range of 461–750 s. The green data points are from *Swift*-UVOT (Perley et al. 2013), the blue and gray points come from *Swift*-XRT, and red data correspond to *Fermi*-LAT. The horizontal error bars are energy bins in which the flux is integrated and the vertical ones are $1\sigma$ statistical errors on the count rate. The gray data points correspond to unabsorbed *Swift*-XRT data, while the blue ones are obtained with the assumption of absorption.

et al. 2013; Laskar et al. 2013) that find no jet break, but differs from Maselli et al. (2014), who claim a break of the later time light curve.

We turn to an additional crucial point: to confirm that the X-ray emission of *Episode 3* belongs to the SN ejecta and not the GRB. To do this it is crucial, as already done for other sources (Ruffini et al. 2014c), to determine the presence of a thermal component in the early time of *Episode 3* and infer the temperature and the size of its emitter. By analyzing the XRT data, we find that adding a blackbody component efficiently improves the fit with respect to a single power law from 196 s to 461 s. The corresponding blackbody temperature decreases in that time duration, from 0.5 keV to 0.1 keV, in the observed frame. Figure 7 shows the evolution of the power law plus blackbody spectra in three time intervals. Clearly the flux of the thermal component drops with time, and the temperature corresponding to the peak flux energy decreases. Kouveliotou et al. (2013) found that a single power law is enough to fit the *NuStar* data in the *NuStar* epochs, and the reason could be that the thermal component has faded away or exceeded the observational capacity of the *Swift* satellite in the *NuStar* epochs, which start later than $10^5$ s.

By assuming that the blackbody radiation is isotropic in the rest frame, the emitter radius along the line of sight increases from $\sim 0.7 \times 10^{13}$ cm at 196 s to $\sim 2.8 \times 10^{13}$ cm at 461 s in the observed frame. This is orders of magnitude smaller than the emission radius of the GRB, which is larger than $10^{15}$ cm in the traditional GRB collapsar afterglow model. The size of $10^{13}$ cm at hundreds of seconds is consistent with the observation of supernova ejecta. After considering the cosmological and the relativistic corrections, $t_a^d \simeq t(1+z)/2\Gamma^2$, where $t$ and $t_a^d$ are the time in the laboratory and observed frame, respectively, and $\Gamma$ is the Lorentz factor of the emitter, we get an expansion speed of $\sim 0.8c$, corresponding to Lorentz factor $\Gamma = 1.67$. These results contradict the considerations inferred in Maselli et al. (2014) $\Gamma \sim 500$, which invoke a value of the Lorentz factor in the traditional collapsar afterglow model (see, e.g., Mészáros 2006). Again, in the prototypical GRB 090618, the Lorentz factors ($1.5 \leqslant \Gamma \leqslant 2.19$) and emission radii ($\sim 10^{13}$ cm) are very similar to those of GRB 130427A presented in Ruffini et al. (2014c). It is interesting that such a thermal component has been also found in the early parts of *Episode 3* of GRB 060729 (adopted in Figure 4) and many other SN associated GRBs (see Ruffini et al. 2014c; Grupe et al. 2007; Starling et al. 2012).

### 3.4. Discussion of Multi-Wavelength Observations in Episode 3

Now we turn to the most unexpected feature in the analysis of the optical, X-ray, $\gamma$-ray, and very high energy emission

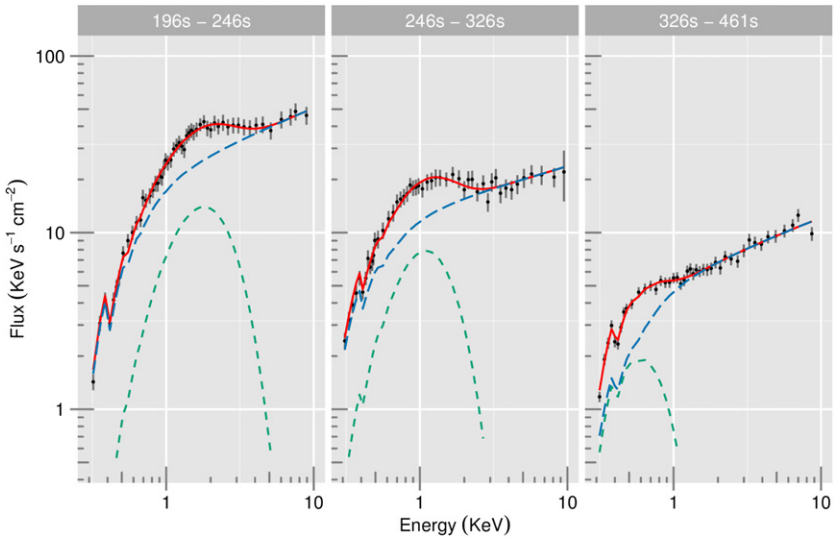


**Figure 7.** Spectral fitting of three time intervals (196 s–246 s, 246 s–326 s, and 326 s–461 s) in *Episode 3*; the data come from *Swift*-XRT (0.3 KeV–10 KeV, without pile-up area). Black points are the deduced data, the green dashed line presents the thermal component, the blue long-dashed line is the power law component, and the red line shows the combination of these two components. Clearly the flux of thermal component drops and the temperature decreases with time.

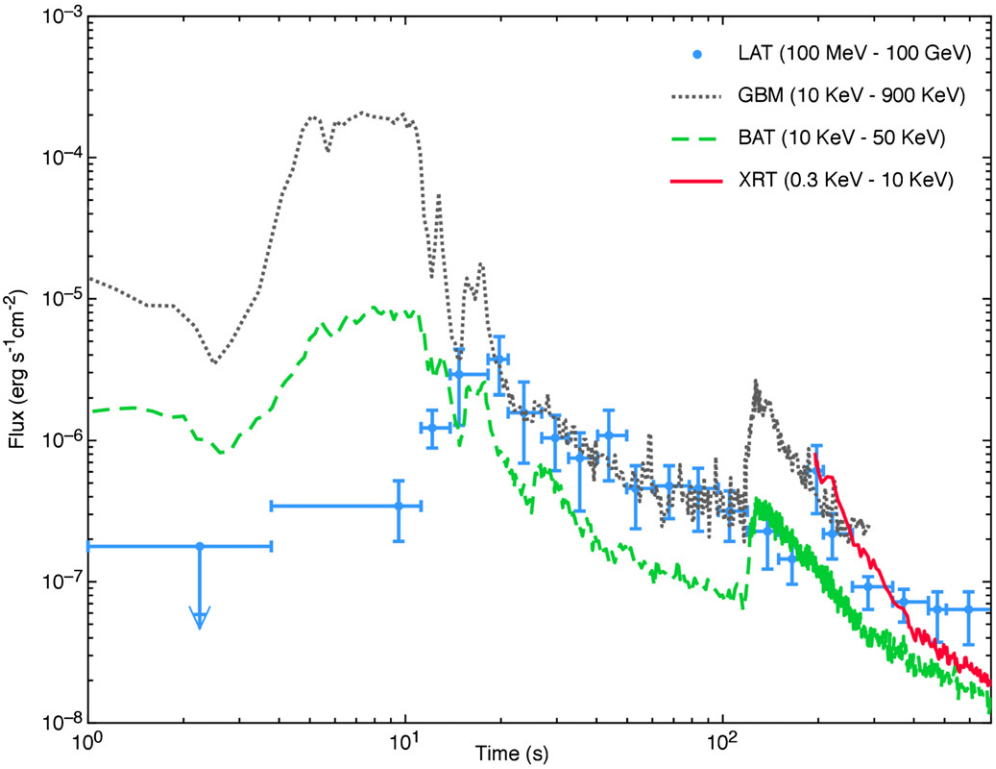


**Figure 8.** Flux of first 700 s. Blue points are the *Fermi*-LAT high energy emission from 100 MeV until 100 GeV (Ackermann et al. 2013), the gray dotted line represents the *Fermi*-GBM from 10 keV to 900 keV, the green dashed line represents the photons detected by *Swift* BAT from 10 keV to 50 keV, and the red solid line is the soft X-ray *Swift*-XRT detection in the range of 0.3–10 KeV. This figure clearly shows that the *Fermi*-LAT emission reaches highest fluence at about 20 s, while the gamma-ray detected by *Fermi*-GBM releases most of the energy within the first 10 s.

in *Episode 3* of GRB 130427A. The optical emission was observed by *Swift*-UVOT and many ground-based telescopes (the *R*-band as an example for the optical observation). The soft X-ray radiation was observed by *Swift*-XRT (0.3–10 keV). Similarly, the hard X-ray radiation was observed by *Swift*-BAT (15–150 keV) and *NuStar* (3–79 keV). The $\gamma$-ray radiation was observed by *Fermi*-GBM (8 KeV –40 MeV), and the high energy radiation by *Fermi*-LAT (100 MeV–100 GeV). The main result is that strong analogies are found in the late emission at all wavelengths in *Episode 3*. After 400 s these luminosities show a common power law behavior with the same constant index as in the X-ray (and clearly with different normalizations), so by fitting multi-wavelength light curves together we have a power law index $\alpha = -(1.3 \pm 0.1)$.

Turning now to the spectrum, integrated between 461 s and 750 s, the energy range covers 10 orders of magnitude, and the best fit is a broken power law (see Figure 6). In addition to the traditional requirements for the optical supernova emission in *Episode 4*, and the much more energetically demanding requirement for the general multi-wavelength emission of *Episode 3* has to be addressed.

### 3.5. The Onset of Episode 3

In the previous sections we emphasized the clear evidence of GeV emission and its analogy in the late power law luminosities as functions of the arrival time for the X-ray, optical, and GeV emissions. Equally important in this section is to emphasize some differences between the X-ray, $\gamma$-ray, and the high energy GeV emission, especially with respect to the onset of *Episode 3* at the end of prompt emission in *Episode 2* (see Figure 8). We observe:

1. The $\gamma$-ray light curves observed by *Fermi*-GBM and hard X-ray observed by *Swift*-BAT have similar shapes. They reach the highest luminosity between 4 s and 10 s during the prompt emission phase of *Episode 2*.
2. The high energy (>100 MeV) GeV emission gradually rises, just after the $\gamma$- and X-ray prompt emissions drop down at the end of *Episode 2*: the high energy GeV emission raises to its peak luminosity at about 20 s. The turn on of the GeV emission coincides, therefore, with the onset of our *Episode 3*. These considerations were recently confirmed and extended by the earliest high energy observations in GRB 090510 (Ruffini et al. 2014, in preparation).
3. At about 100 s, the *Swift*-XRT starts to observe the soft X-ray and a sharp spike appears in the hard X-ray and gamma ray bands (see Figure 8). Only at this point does the *Swift*-XRT start to observe soft X-ray. We are currently addressing the occurrence of the spike to the thermal emission observed to follow in the sharp decay of the X-ray luminosity prior to the plateau and the above mentioned common power law decay (Ruffini et al. 2014b).

The detailed analysis of the prolonged emission observed by *Fermi*-LAT in GeV enables us to set specific limits on the Lorentz factor of this high energy emission. We analyzed the GeV emission from ~300 s to $2.5 \times 10^4$ s, dividing the time interval into seven sub-intervals and in each of them collecting the corresponding maximum photon energy and photon index of the spectral energy distribution, as shown in Ackermann et al. (2013, Figure 2). We focused our attention on the estimate of the Lorentz factor for this high energy component from the usual optical depth formula for pair creation $\tau_{\gamma\gamma}$ (see, e.g., Lithwick & Sari 2001; Gupta & Zhang 2008). We computed, for

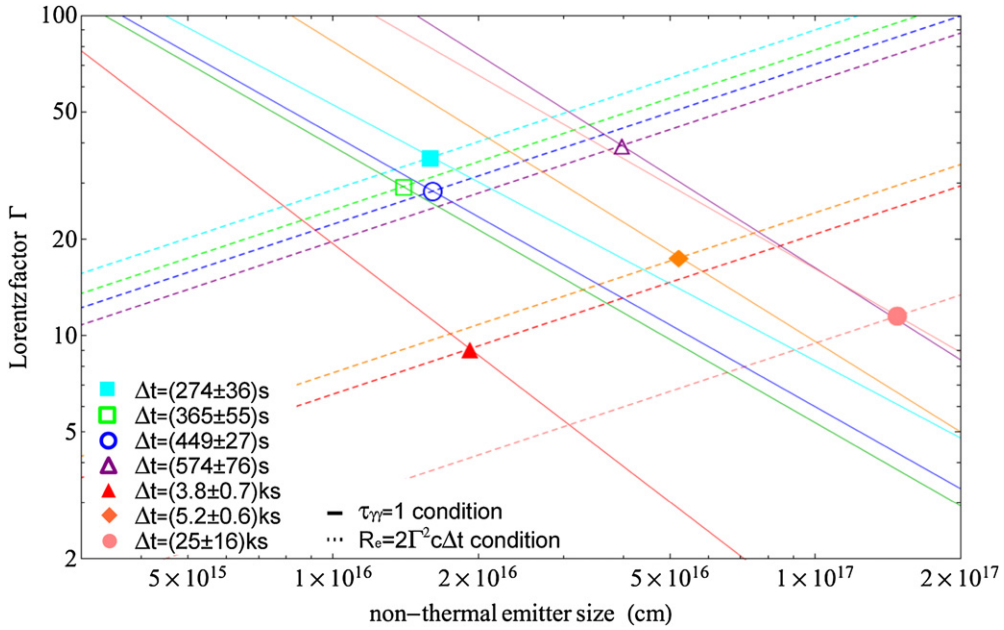


**Figure 9.** Constraints on the Lorentz factors and the size of the GeV emitting region at the transparency point. Solid curves represent the curves defined by varying the emitting region size from the $\tau_{\gamma\gamma} = 1$ condition; dot-dashed curves represent the radius of the emitter obtained from causality in the ultrarelativistic regime (i.e., $R_{em} = 2\Gamma^2 c\Delta t$). Filled circles correspond to the solutions of both limits. The different colors refer to the time intervals from ∼273 s to 24887 s, in the order cyan, green, blue, purple, red, orange, and pink, respectively.

different values of radii of the emitter, the corresponding Lorentz factors at the transparency condition (i.e., $\tau_{\gamma\gamma} = 1$; see the solid curves in Figure 9). The constraints on the size of the emitting regions come from causality in the ultrarelativistic regime (i.e., $R_{\rm em} = 2\Gamma^2 c\Delta t$), where $\Delta t$ corresponds to the duration of the time intervals under consideration (see the dot-dashed curves in Figure 9). The values of the Lorentz factor range between ∼10 and ∼40, and correspondingly, the radii of the emitting region at the transparency point are located between $\sim 10^{16}$ cm and $\sim 2 \times 10^{17}$ cm (see the filled circles in Figure 9).

### *3.6. General Considerations on Recent Theoretical Progress on BdHD*

The concurrence of the above well-defined scaling laws and power law of the observed luminosities both in the X-ray and/or in the optical domains in *Episode 3* of GRB 130427A have been considered arguments in favor of looking to the *r*-process and to heavy nuclei radioactive decay as the energy sources (Ruffini et al. 2014c; see the pioneering work of Li & Paczynski 1998). The extended interaction of the $\nu$-NS and its binary NS companion in the SN ejecta provides an environment for *r*-processes to create the needed neutron-rich very heavy elements to attribute some of the electromagnetic energy in *Episode 3* to nuclear decay, $\approx 10^{52}$ erg. Alternatively, we are considering emission originating from type-I and type-II Fermi acceleration mechanisms, which are introduced by Fermi precisely to explain the radiation process in the SN remnants (Fermi 1949). In addition these processes can lead to a power law spectrum (Aharonian 2004) that is similar to that presented in this paper and our recent letter (Ruffini et al. 2014c). The GRB emission of *Episode 2* interacting with the SNe ejecta could represent the energy injection long sought by Fermi for the onset of his acceleration mechanism (Fermi 1949).

Both of these processes can operate as energy sources for the mildly relativistic X-ray component and the relativistic GeV emission of *Episode 3*.

We are currently examining additional BdHN sources and giving particular attention to understanding the highest GeV energy emission, which is unexpected in the traditional *r*-process. The inferred Γ Lorentz factor for the GeV emission points to the possibility of a direct role of the two remaining components in the IGC paradigm: the newly born neutron star ($\nu$NS) and the just born black hole (see Figure 1). There is also the distinct possibility that these two systems have become members of a newly born binary system[12] (Rueda & Ruffini 2012).

## 4. CONCLUSION

We recall that GRB 130427A is one of the most energetic GRBs ever observed ($E_{\rm iso} \simeq 10^{54}$ erg), with the largest $\gamma$-ray fluence and the longest lasting simultaneous optical, X-ray, $\gamma$-ray, and GeV observations of the past 40 yr. For this reason we performed our own data analysis of the *Swift* and *Fermi* satellites (see Sections 3) in order to probe the BdHN nature of this source (see Section 3.3) and infer new perspectives for the IGC paradigm and the physical and astrophysical understanding of GRB.

We summarize the main results by showing how the analysis of GRB 130427A should be inserted in a wider context with three different areas: (1) the formulation and the observational consequences of the IGC paradigm; (2) the comprehension induced by the multi-wavelength observations of GRB130427A; and (3) the BDHN versus HN properties. BDHN is relevant in establishing a new alternative distance indicator in astrophysics, which will be summarized in the following.

With reference to the formulation and observational consequences of the IGC paradigm:

1. The IGC paradigm introduces a new experience in astrophysics that has been successfully applied in particle

[12] Presentation of R. Ruffini in Yerevan: http://www.icranet.org/images/stories/Meetings/meetingArmenia2014/talks/ruffini-1.pdf

physics: to understand that a system traditionally considered elementary is actually a composed system, and that new components in the system can appear from the influence of collisions or decay. Well-known physical examples are represented by the introduction of the quark (Aad et al. 2012), or the creation of new particles in a decay or collision of elementary particle system: the Fermi theory of beta decay or the mesons production in electron positron collision in storage rings are classical examples. These facts are routinely accepted in particle physics, although Fermi had to explain them at the time (Fermi 1934). In astrophysics this situation is new. To see that a process until recently considered elementary, such as the GRB, does contain four different astrophysical systems, and that the interaction between two of them (i.e., the FeCO core undergoing SN and the companion NS binary) give rise to two different new systems, a $\nu$NS and a BH, and that the entire process occurs in less than 200 s, is a totally new condition. To understand it, a new technical and conceptual approach is needed. The new style of research is more similar to that adopted in particle physics than in classical astronomy; see Figure 1.

2. Possibly the most profound novelty in this approach, for the understanding of GRBs, is the introduction of the four episodes that are summarized in Section 1. The traditional GRB description corresponds to *Episode 2*. *Episode 1* corresponds to the dynamical accretion of the SN ejecta onto the companion NS. We are now considering an enormous rate of accretion of $10^{31}$ g s$^{-1}$, which is $10^{15}$ times larger than that usually considered in the binary X-ray source in systems like Centaurus X-3 or Cygnus X-1 (see e.g., in Giacconi & Ruffini 1975). This process opened a new field of research by presenting the first realization of the hypercritical accretion introduced by Bondi–Hoyle–Littleton, as well as the testing ground of the neutrinos emission pioneered in the Zel'dovich et al. (1972) and Ruffini & Wilson (1975) (see Section 1). The pure analytic simplified solutions in Rueda & Ruffini (2012) are now supported by direct numerical simulation in Fryer et al. (2014, and Figure 1 therein).
3. The main revolution of the IGC paradigm for GRBs comes from the discovery of the universal laws discovered in *Episode 3*, which compare the explosive, irregular phases, varying from source to source in all observed GRBs in *Episode 1* and *Episode 2*. The universality of *Episode 3*, as well as the precise power laws and scaling laws discovered, changes the field of GRB analysis by making it one of time-resolved, high-precision, and reproducible measurements. Additional unexplored physical phenomena occurs in *Episode 3*, adding to the new ultrarelativistic regimes already observed in the *Episode 2* in previous years,[13] see Figure 3 and Figure 4 as well as Figure 5.

With reference to the comprehension induced by the multi-wavelength observations of GRB130427:

1. Following the work on the *GS* (Pisani et al. 2013) and the more recent work on the nested structures (Ruffini et al. 2014c), we have first verified that the soft X-ray emission of GRB 130427A follows for time $t \simeq 10^4$ s the power law decay described in Pisani et al. (2013). Surprisingly, this most energetic GRB unveils that such power law behavior as already exists at the early time as t $\sim$100 s (details in Ruffini et al. 2014c). From the X-ray thermal component observed at the beginning of *Episode 3* following a spiked emission at $\sim$100 s, a small Lorentz factor of the emitter is inferred ($\Gamma < 2$). This X-ray emission appears to originate in a mildly relativistic regime with a velocity $v \sim 0.8c$, does not appear to have substantial beaming, and appears to be relatively symmetric with no jet break; see Figure 5 and Ruffini et al. (2014c, Figure 2).
2. We made a multi-wavelength analysis of *Episode 3* where we compared optical data from *Swift*-UVOT and ground-based telescopes, X-ray data from *Swift*-XRT, $\gamma$-ray data from *Fermi*-GBM, and very high energy data in the GeV from *Fermi*-LAT. The high energy emission appears to be detectable at the end of the prompt radiation phase in *Episode 2*, when the fluence of the X-ray and $\gamma$-ray of the prompt exponentially decreases and becomes transparent for the very high energy photons in the *Fermi*-LAT regime. From the transparency condition of the GeV emission, a Lorentz Gamma factor of 10–40 is deduced. In principle this radiation, although no brake is observed in its power law, could be in principle beamed; see Figure 9.
3. Although the light curves of X-ray and GeV emission appear to be very similar, sharing similar power law decay index, their Lorentz $\Gamma$ factors appear to be very different, and their physical origins are necessarily different. Within the IGC model, the X-ray and high energy can originate from the interaction of some of the physical components (e.g., neutron star and black hole) that were newly created in the C-matrix: the interaction of the GRBs with the SN ejecta (Ruffini et al. 2014b) may well generate the X-ray emission and the associated thermal component. The high energy should be related to the novel three components (i.e., the BH, the $\nu$NS, and the SN ejecta). From the dynamics it is likely that the $\nu$NS and the BH form a binary system (see e.g., Rueda & Ruffini 2012 and the presentation by one of the authors).[14]

With reference to the BDHN versus HN properties:

1. The verification of the BdHN paradigm in GRB 130427A has confirmed that for sources with isotropic energy approximately $10^{54}$ erg, the common power law behavior is attained at earlier times (i.e., $\sim 10^3$ s) and higher X-ray luminosities than the characteristic timescale indicated in (Pisani et al. 2013) (see Figure 3). From the observation of the constant-index power law behavior in the first $2 \times 10^4$ s of the X-ray luminosity light curve, which overlap with the known BdHNe, it is possible to estimate the redshift of the source, the isotropic energy of the GRB, and the fulfillment of the necessary and sufficient condition for predicting the occurrence of the SN after $\sim$10 days in the rest frame of the source (see, e.g., GCN 14526). This procedure has been successfully applied to GRB 140512A (R. Ruffini et al., in preparation).
2. The overlap with the *GS* members of the late X-ray emission observed by the *Swift* XRT, referred to as the rest frame of the source, introduces a method to establish an independent distance estimator of the GRBs. Although this method has been amply applied (e.g., GRBs 060729, 061007, 080319, 090618, 091127, 111228A), we also declare that there are some clear outliers to this phenomenon, such as GRB 060614 (Ruffini et al. 2013a), 131202A (Ruffini et al.

[13] Presentation of R. Ruffini in the 13th Marcel Grossmann Meeting: http://www.icra.it/mg/mg13

[14] Presentation of R. Ruffini in Yerevan: http://www.icranet.org/images/stories/Meetings/meetingArmenia2014/talks/ruffini-1.pdf

2013c), and 140206A (Ruffini et al. 2014a). These are all cases of great interest and the solution of this contradiction may be of particular astrophysical significance. Particularly interesting is the case of GRB 060614 because the cosmological redshift has not been directly measured and there can be a misidentification of the host galaxy (Cobb et al. 2006).

3. As first pointed out in Rueda & Ruffini (2012) and Ruffini et al. (2014c), and further evidenced in Fryer et al. (2014), the crucial factor that may explain the difference between *family 1* and *family 2* GRBs is the initial distance between the FeCO core and its binary NS companion. The accretion from the SN ejecta onto the companion NS, and the consequent emission process decrease, by increasing this distance has consequently hampered the possibility for the binary companion NS to reach its critical mass (see Figures 3 and 4 in Izzo et al. 2012, and the discuss therein). Unlike *family 2*, in *family 1* no BH is formed, no GRB is emitted, and neither *Episode 2* nor *Episode 3* exists—only a softer and less energetic radiation from the accretion onto the neutron star will be observed in these sources. The problem of explaining the coincidence between the GRB and supernova in the case of *family 1* is just a tautology: no GRB in this family exists, only a hypernova (Ruffini et al. 2014c).

This paper addresses recent results on the IGC paradigm applied to long GRBs. The IGC paradigm and the merging of binary neutron stars has also been considered for short GRBs (see e.g., Muccino et al. 2013a, 2013b, 2014; Ruffini et al. 2014c) and is now being further developed.

We acknowledge the use of public data from the *Swift* and *Fermi* data archive. We thank Robert Jantzen for his careful reading and valuable advice. We also thank the editor and the referee for their constant attention and beneficial suggestions, which largely improve this paper. M.E., M.K., and G.B.P. are supported by the Erasmus Mundus Joint Doctorate Program by Grant Numbers 2012-1710, 2013-1471, and 2011-1640, respectively, from the EACEA of the European Commission.

## REFERENCES

Aad, G., Abajyan, T., Abbott, B., et al. 2012, PhLB, 716, 1
Ackermann, M., Ajello, M., Asano, K., et al. 2013, Sci, 343, 42
Aharonian, F. A. 2004, Very High Energy Cosmic Gamma Radiation: A Crucial Window on the Extreme Universe (Singapore: World Scientific Publishing)
Bernardini, C. 2004, PhP, 6, 156
Bloom, J. S., Perley, D. A., Li, W., et al. 2009, ApJ, 691, 723
Bondi, H. 1952, MNRAS, 112, 195
Bondi, H., & Hoyle, F. 1944, MNRAS, 104, 273
Broderick, A. E. 2005, MNRAS, 361, 955
Cobb, B. E., Bailyn, C. D., van Dokkum, P. G., & Natarajan, P. 2006, ApJL, 651, L85
de Ugarte Postigo, A., Xu, D., Leloudas, G., et al. 2013, GCN Circ., 14646
Evans, P. A., Beardmore, A. P., Page, K. L., et al. 2007, A&A, 469, 379
Evans, P. A., Beardmore, A. P., Page, K. L., et al. 2009, MNRAS, 397, 1177
Fermi, E. 1934, Il Nuovo Cimento, 11, 1
Fermi, E. 1949, PhRv, 75, 1169
Flores, H., Covino, S., Xu, D., et al. 2013, GCN Circ., 14491
Friis, M., & Watson, D. 2013, ApJ, 771, 15
Fryer, C. L., Benz, W., & Herant, M. 1996, ApJ, 460, 801
Fryer, C. L., Rueda, J. A., & Ruffini, R. 2014, ApJ, 793, L36
Fryer, C. L., Woosley, S. E., & Hartmann, D. H. 1999, ApJ, 526, 152
Galama, T. J., Vreeswijk, P. M., van Paradijs, J., et al. 1998, Natur, 395, 670
Giacconi, R., & Ruffini, R. 1975, Physics and Astrophysics of Neutron Stars and Black Holes (Amsterdam: North Holland Publishing Co.)
Grupe, D., Gronwall, C., Wang, X.-Y., et al. 2007, ApJ, 662, 443
Guetta, D., & Della Valle, M. 2007, ApJL, 657, L73
Gupta, N., & Zhang, B. 2008, MNRAS, 384, L11
Izzo, L., Rueda, J. A., & Ruffini, R. 2012, A&A, 548, L5
Kouveliotou, C., Granot, J., Racusin, J. L., et al. 2013, ApJL, 779, L1
Kovacevic, M., Izzo, L., Wang, Y., et al. 2014, A&A, 569, A108
Laskar, T., Berger, E., Zauderer, B. A., et al. 2013, ApJ, 776, 119
Levan, A. J., Cenko, S. B., Perley, D. A., & Tanvir, N. R. 2013a, GCN Circ., 14455
Levan, A. J., Fruchter, A. S., Graham, J., et al. 2013b, GCN Circ., 1468
Levan, A. J., Tanvir, N. R., Fruchter, A. S., et al. 2014, ApJ, 792, 115
Li, L.-X., & Paczynski, B. 1998, ApJL, 507, L59
Lithwick, Y., & Sari, R. 2001, ApJ, 555, 540
Maselli, A., Beardmore, A. P., Lien, A. Y., et al. 2013, GCN Circ., 14448
Maselli, A., Melandri, A., Nava, L., et al. 2014, Sci, 343, 48
Mészáros, P. 2006, RPPh, 69, 2259
Muccino, M., Ruffini, R., Bianco, C. L., Izzo, L., & Penacchioni, A. V. 2013a, ApJ, 763, 125
Muccino, M., Ruffini, R., Bianco, C. L., et al. 2013b, ApJ, 772, 62
Muccino, M., Bianco, C. L., Izzo, L., et al. 2014, GrCo, 20, 197
Nava, L., Sironi, L., Ghisellini, G., Celotti, A., & Ghirlanda, G. 2013, MNRAS, 433, 2107
Nousek, J. A., Kouveliotou, C., Grupe, D., et al. 2006, ApJ, 642, 389
Page, K. L., Starling, R. L. C., Fitzpatrick, G., et al. 2011, MNRAS, 416, 2078
Penacchioni, A. V., Ruffini, R., Bianco, C. L., et al. 2013, A&A, 551, A133
Penacchioni, A. V., Ruffini, R., Izzo, L., et al. 2012, A&A, 538, 58
Perley, D. A., Cenko, S. B., Corsi, A., et al. 2013, ApJ, 781, 37
Pian, E., Amati, L., Antonelli, L. A., et al. 2000, ApJ, 536, 778
Piran, T. 2005, RMP, 76, 1143
Pisani, G. B., Izzo, L., Ruffini, R., et al. 2013, A&A, 552, L5
Rhoads, J. E. 1999, ApJ, 525, 737
Romano, P., Campana, S., Chincarini, G., et al. 2006, A&A, 456, 917
Rueda, J. A., & Ruffini, R. 2012, ApJL, 758, L7
Ruffini, R., Bernardini, M. G., Bianco, C. L., et al. 2008, in 11th Proc. Marcel Grossmann Meeting (Singapore: World Scientific Publishing), 368
Ruffini, R., Bianco, C. L., Enderli, M., et al. 2013a, GCN Circ., 15560, 1
Ruffini, R., Bianco, C. L., Enderli, M., et al. 2013b, GCN Circ., 14526
Ruffini, R., Bianco, C. L., Enderli, M., et al. 2013c, GCN Circ., 15576, 1
Ruffini, R., Bianco, C. L., Enderli, M., et al. 2014a, GCN Circ., 15794, 1
Ruffini, R., Bianco, C. L., Fraschetti, F., Xue, S.-S., & Chardonnet, P. 2001, ApJ, 555, L117
Ruffini, R., Izzo, L., Muccino, M., et al. 2014b, A&A, 569, A39
Ruffini, R., Muccino, M., Bianco, C. L., et al. 2014c, A&A, 565, L10
Ruffini, R., Salmonson, J. D., Wilson, J. R., & Xue, S.-S. 1999, A&A, 350, 334
Ruffini, R., Salmonson, J. D., Wilson, J. R., & Xue, S.-S. 2000, A&A, 359, 855
Ruffini, R., & Wilson, J. R. 1975, PhRvD, 12, 2959
Starling, R. L. C., Page, K. L., Pe'er, A., Beardmore, A. P., & Osborne, J. P. 2012, MNRAS, 427, 2950
Tanvir, N. R., Rol, E., Levan, A. J., et al. 2010, ApJ, 725, 625
Tavani, M. 1998, ApJL, 497, L21
Trotter, A., Reichart, D., Haislip, J., et al. 2013, GCN Circ., 1466
van Eerten, H. J., & MacFadyen, A. I. 2012, ApJ, 751, 155
van Eerten, H. J., Zhang, W., & MacFadyen, A. 2010, ApJ, 722, 235
von Kienlin, A. 2013, GCN Circ., 14473
Woosley, S. E. 1993, ApJ, 405, 273
Xu, D., de Ugarte Postigo, A., Leloudas, G., et al. 2013, ApJ, 776, 98
Xu, D., de Ugarte Postigo, A., Schulze, S., et al. 2013, GCN Circ., 14478
Zel'dovich, Y. B., Ivanova, L. N., & Nadezhin, D. K. 1972, SvA, 16, 209